

Capillary Hysteresis and Gravity Segregation in Two Phase Flow Through Porous Media

K. Mitra^{*1} and C.J. van Duijn^{2,3}

¹*Radboud University, Faculty of Science*

²*Eindhoven University of Technology, Department of Mechanical Engineering*

³*Utrecht University, Department of Earth Sciences*

Abstract

We study the gravity driven flow of two fluid phases in a one dimensional homogeneous porous column when history dependence of the pressure difference between the phases (capillary pressure) is taken into account. In the hyperbolic limit, solutions of such systems satisfy the Buckley-Leverett equation with a non-monotone flux function. However, solutions for the hysteretic case do not converge to the classical solutions in the hyperbolic limit in a wide range of situations. In particular, with Riemann data as initial condition, stationary shocks become possible in addition to classical components such as shocks, rarefaction waves and constant states. We derive an admissibility criterion for the stationary shocks and outline all admissible shocks. Depending on the capillary pressure functions, flux function and the Riemann data, two cases are identified a priori for which the solution consists of a stationary shock. In the first case, the shock remains at the point where the initial condition is discontinuous. In the second case, the solution is frozen in time in at least one semi-infinite half. The predictions are verified using numerical results.

1 Introduction

In this paper we investigate gravity driven flow of two fluid phases through a homogeneous one-dimensional porous column. We are concerned with the special case in which the length of the column is large and no injection of fluid is present (i.e. the total flow is zero). The corresponding mathematical model uses the well-known Buckley-Leverett equation, see [9]. In dimensionless form it reads

$$\partial_t S + \partial_x h(S) = 0. \tag{1.1}$$

^{*}Corresponding author: email: koondanibha.mitra@ru.nl

Here $S \in [0, 1]$ is the saturation of the wetting phase and $h : [0, 1] \rightarrow [0, \infty)$ the fractional flow function of which a typical sketch is shown in Figure 1 (left). The space coordinate is x and t denotes time. We solve (1.1) for $t > 0$ and $x \in \mathbb{R}$, where we prescribe at $t = 0$ the Riemann condition

$$S(x, 0) = \begin{cases} S_T & \text{for } x < 0, \\ S_B & \text{for } x > 0, \end{cases} \text{ where } 0 < S_B < S_T < 1 \text{ are constants.} \quad (1.2)$$

Solutions of (1.1)–(1.2) are generally non-unique [14, Chapter 1]. To find the physically relevant solution, we replace (1.1) by the capillary Buckley-Leverett equation

$$\partial_t S + \partial_x [h(S)(1 + \delta \partial_x p)] = 0. \quad (1.3)$$

and study the limit $\delta \rightarrow 0$. In (1.3), p is the pressure difference between the fluid phases and δ is the dimensionless capillary number which scales inversely with the length of the domain (reference length). Hence for large domains, (1.1) is approximated by (1.3). A detailed derivation is given in Section 2.

To solve (1.3) a relation between S and p is assumed. In the standard equilibrium approach, one uses

$$p = p_c(S), \quad (1.4)$$

where $p_c : (0, 1] \rightarrow [0, \infty)$ is a capillary pressure function [9].

For $\delta > 0$, let (S_δ, p_δ) denote the solution of (1.2)–(1.4). The hyperbolic limit as $\delta \rightarrow 0$ yields the well known Buckley-Leverett solution of (1.1)–(1.2), comprising of constant states separated by shocks and rarefaction waves [14, 15, 23]. In particular, shocks can be seen as the limit of smooth, monotone travelling waves which become steeper as $\delta \rightarrow 0$ [14, 15, 32]. It is also known that the hyperbolic limit solution is independent of the actual shape of the capillary pressure p_c as long as the approximating equation (1.3) is of convection-diffusion type [14, Chapter 3].

However, there are other more realistic capillary pressure expressions for which the limiting ($\delta \rightarrow 0$) solution does inherit some properties of the vanishing capillarity. This was studied in detail in [19, 31, 33, 35] for the case where (1.4) is replaced by the non-equilibrium expression

$$p = p_c(S) - \tau \partial_t S,$$

where $\tau > 0$ is a relaxation parameter called dynamic capillarity coefficient which attributes to saturation overshoots [17, 21, 34].

In this paper we investigate the effect of hysteresis in the capillary pressure. Since $p_c(\cdot)$ is a single valued function of saturation only, it does not contain any information about the history or directionality of the process. In particular, it does not distinguish between imbibition and drainage. No hysteretic effects are present in (1.4). However, hysteresis is known to occur in multi-phase porous media flow. This was first observed by Haines in

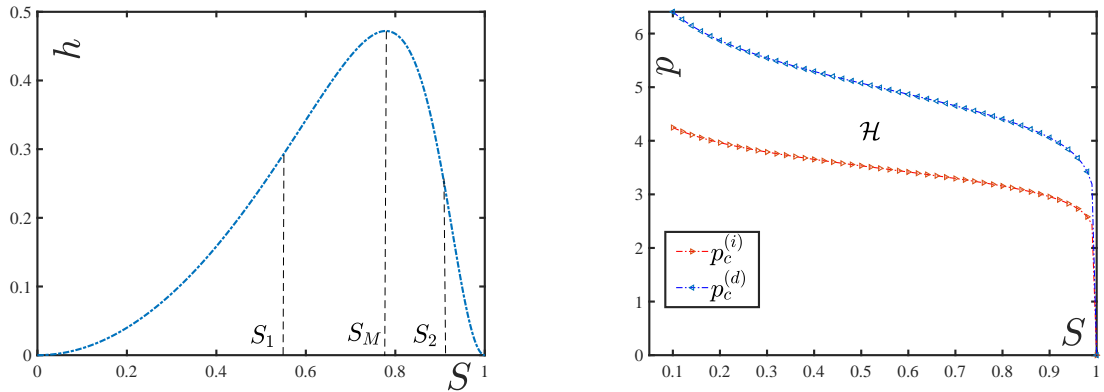


Figure 1: (left) The h - S curve for water (wetting phase, viscosity $5.23 \times 10^{-4}[\text{Pa} \cdot \text{s}]$) and methane (viscosity $1.202 \times 10^{-5}[\text{Pa} \cdot \text{s}]$). In reference to Section 2, the Brooks-Corey relationship has been used for the relative permeabilities, the mobility ratio is $M = 43.52$ and the characteristic saturations S_M , S_1 , S_2 are marked. (right) The imbibition and drainage capillary pressure curves and the hysteretic region \mathcal{H} . The van Genuchten model has been used for $p_c^{(i)}$ and $p_c^{(d)}$. Details are given in the numerical section.

1930 and has been verified since by numerous experiments, some notable examples being [22, 36]. An overview of different hysteresis models from the mathematical, modelling and physical perspectives can be found in [8, 16, 29].

In our approach we replace (1.4) by the following hysteresis description. Let

$$p_c^{(i)}, p_c^{(d)} : (0, 1] \rightarrow [0, \infty), \quad p_c^{(i)}(S) < p_c^{(d)}(S) \text{ for } 0 < S < 1,$$

denote the imbibition and drainage capillary pressure functions, typical examples being shown in Figure 1 (right), and let

$$\mathcal{H} := \{(S, p) : 0 < S \leq 1, p_c^{(i)}(S) \leq p \leq p_c^{(d)}(S)\}$$

be the hysteresis region in the (S, p) -plane, as indicated in Figure 1 (right). We restrict ourselves to the well-known play-type hysteresis model, first proposed in [6], which relates S and p via the relation

$$p \in \mathcal{H}, \text{ and } p = \begin{cases} p_c^{(i)}(S) & \text{when } \partial_t S > 0, \\ \in [p_c^{(i)}(S), p_c^{(d)}(S)] & \text{when } \partial_t S = 0, \\ p_c^{(d)}(S) & \text{when } \partial_t S < 0. \end{cases} \quad (1.5)$$

The play-type model assumes that switching from drainage to imbibition, or vice versa, occurs only along vertical scanning curves. For the rest of the study, the state when $\partial_t S = 0$ and consequently $p \in [p_c^{(i)}(S), p_c^{(d)}(S)]$ will be referred to as the undetermined

state of the system, whereas $\partial_t S > 0$ (consequently $p = p_c^{(i)}(S)$) and $\partial_t S < 0$ ($p = p_c^{(d)}(S)$) will refer to the imbibition and drainage states, respectively. Other models, such as the Lenhard-Parker model [24] and the extended play-type hysteresis model [8, 18] assume a more complex relation between S and p when $p_c^{(i)}(S) < p < p_c^{(d)}(S)$. We comment on the consequences of such models in Remark 4.3.

The purpose of this paper is to construct solutions of the Riemann problem (1.1)–(1.2) that arise as the hyperbolic limit ($\delta \rightarrow 0$) of (1.2)–(1.3) and (1.5). We demonstrate that the occurrence of hysteresis in the vanishing capillary term, i.e. using (1.5) instead of (1.4), gives solutions that are significantly different, specially when S_B is close to 0 and S_T is close to 1. In particular, a stationary discontinuity occurs at the location where the initial condition is discontinuous. This is illustrated in Figure 2. The magnitude of the jump depends on the difference $p_c^{(d)}(S) - p_c^{(i)}(S)$, as will be discussed later. This behaviour

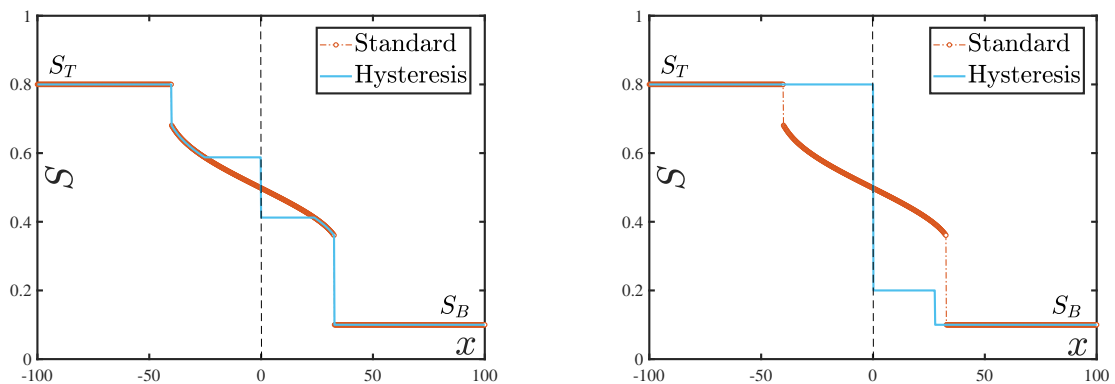


Figure 2: Vanishing capillarity solutions of (1.1) with initial condition (1.2). Here, $S_B = 0.1$, $S_T = 0.8$ and $t = 100$. The red marked profiles show the classical solutions (for the standard model (1.4)), whereas, the blue solid profiles show the result for the play-type model (1.5). For the (left) plot, $p_c^{(i)}$ and $p_c^{(d)}$ curves are close to each other, whereas in the (right) plot the curves are as shown in Figure 1 (right). Exact details are given later.

was mentioned briefly in Section 3.5 of [19]. A stationary discontinuity in saturation for the classical problem (with no hysteresis) was also predicted in [2] at the interface between two semi-infinite halves having different h and p_c functions. However, the directionality imposed by hysteresis demands an extension of their results. The saturation discontinuity has major practical importance as the saturation distribution can change considerably if hysteresis is present, as is evident from Figure 2.

Remark 1.1 (Vanishing capillarity method). *In the mathematical literature, the method of finding solutions of equations such as (1.1) by passing to the limit $\delta \rightarrow 0$ in (1.3) is called the vanishing viscosity method, and was studied in classical references such as*

[13, 23]. In these papers, the notion of entropy was introduced as well. In their context, the vanishing viscosity solution is the entropy solution. In our application, the meaning of entropy is not clear. Renaming viscosity as capillarity, we thus rely on the vanishing capillarity method. We call the approximate solutions (S_δ, p_δ) for $\delta > 0$ the capillarity solutions, and the $\delta \rightarrow 0$ limit solution the vanishing capillarity solution.

Hysteresis models have been analysed exhaustively, particularly in one spatial dimension [17]. Existence and uniqueness results for the regularised play-type model are given in [10, 12, 18, 28] and [7] respectively. A horizontal redistribution study using similarity solutions was performed in [8]. Travelling wave analysis for hysteresis was conducted for flow of water through soil in [5, 20, 21, 34]. For the two-phase case, travelling waves were studied in [19] for monotone flux functions and vanishing capillarity solutions were derived that differ significantly from the classical ones. These solutions were used to explain the observation of stable and growing saturation plateaus in infiltration experiments. Non-classical solutions for non-monotone flux functions like h were investigated in [30], although hysteresis was not included. In [11], examples of how hysteresis influences hyperbolic solutions in mechanics are found. The role of relative permeability hysteresis, which is not addressed in this study, in determining the hyperbolic solutions is examined in [1, 4, 26, 27]. However, the relation between p and S is assumed to be a linear one in these articles. In the current study, we investigate the vanishing capillarity solutions for the capillary hysteresis models in the non-monotone flux case and show that non-classical behaviour such as stationary shocks may occur. Stationary discontinuities have been studied in [2] for heterogeneous media without hysteresis and for redistribution problems (no gravity) in [8, 25] with hysteresis. The occurrence of a stationary discontinuity due to hysteresis in gravity driven flows is to our knowledge a novel observation.

We structure the paper as follows: In Section 2 the assumptions are stated and the model is derived. Using travelling wave analysis, all admissible shocks, including stationary shocks, are derived in Section 3 for the standard and the hysteresis model. Then, in Section 4, the admissible shocks are used to construct the vanishing capillarity solutions. Two cases are identified when the solutions for hysteresis deviate from the classical ones. This is determined a priori from h , $p_c^{(i)}$, $p_c^{(d)}$, S_B and S_T . In the first case, the solution has a stationary discontinuity while the rest of the solution retains the structure of the classical solutions (Section 4.2.1). The second case has no classical counterparts and the solution is frozen in one of the semi-infinite halves (Section 4.2.2). Finally, in Section 5, we solve (1.2)–(1.3) and (1.5) numerically for small $\delta > 0$ and show that the solution closely resembles our predictions.

2 Problem Formulation

We set-up the two-phase flow problem in a one-dimensional homogeneous porous domain. The phases are assumed to be incompressible and immiscible. There is no injection at

the boundaries, making the flow purely counter-current and gravity driven, having zero total flux of the combined wetting and non-wetting phases. Following [9], we consider for each phase the mass balance equation and the corresponding Darcy Law. This yields

$$\phi \partial_t S = \partial_x \left[\frac{K}{\mu_w} k_w(S) (\partial_x p_w - \rho_w g) \right] \quad (\text{wetting phase}), \quad (2.1a)$$

$$\phi \partial_t (1 - S) = \partial_x \left[\frac{K}{\mu_n} k_n(1 - S) (\partial_x p_n - \rho_n g) \right] \quad (\text{non-wetting phase}). \quad (2.1b)$$

For each phase $\alpha = w, n$ (w and n representing the wetting and the non-wetting phases respectively), p_α denotes the pressure, k_α the relative permeability, μ_α the viscosity and ρ_α the density. The porosity ϕ and absolute permeability K are properties of the medium and are constant due to the assumption of homogeneity. Finally, gravity points in the direction of positive x and g is the gravitational constant. For the remainder of the study we assume that the wetting phase is denser than the non-wetting phase, i.e.,

$$\rho_n < \rho_w.$$

Adding the equations in (2.1) gives

$$\partial_x \left[\frac{K k_w}{\mu_w} (\partial_x p_w - \rho_w g) + \frac{K k_n}{\mu_n} (\partial_x p_n - \rho_n g) \right] = 0,$$

The term inside the brackets [] is the total flux of the combined phases. Since no injection takes place in the column

$$\frac{K k_w}{\mu_w} (\partial_x p_w - \rho_w g) + \frac{K k_n}{\mu_n} (\partial_x p_n - \rho_n g) = 0.$$

Defining the capillary pressure and mobility ratio as

$$p := p_n - p_w \quad \text{and} \quad M := \mu_w / \mu_n$$

respectively, one obtains through rearrangement

$$\frac{K k_w}{\mu_w} (\partial_x p_w - \rho_w g) = - \frac{K}{\mu_w} \frac{k_n k_w}{k_n + M^{-1} k_w} \partial_x p - \frac{K g (\rho_w - \rho_n)}{\mu_w} \frac{k_n k_w}{k_n + M^{-1} k_w}. \quad (2.2)$$

To non-dimensionalise (2.1), we introduce a characteristic pressure p_{ref} (taken from the capillary pressure curves), a characteristic length L (length of column or typical observation distance) and a characteristic time t_{ref} . We further define the fractional flow function

$$h := \frac{k_n k_w}{k_n + M^{-1} k_w}, \quad (2.3)$$

and introduce the dimensionless capillary number

$$\delta := \frac{p_{\text{ref}}}{(\rho_w - \rho_n) g L} > 0. \quad (2.4)$$

Inserting (2.2) into (2.1a), choosing $t_{\text{ref}} = \frac{\mu_w \phi L}{Kg(\rho_w - \rho_n)}$, and redefining the dimensional quantities as their dimensionless versions

$$p \mapsto \frac{p}{p_{\text{ref}}}, \quad t \mapsto \frac{t}{t_{\text{ref}}}, \quad x \mapsto \frac{x}{L},$$

one obtains (1.3).

The Brooks-Corey model is commonly used for the relative permeability functions:

$$k_\alpha(S) = S^2 \quad \text{for } \alpha = n, w. \quad (2.5)$$

This gives the shape of h as shown in Figure 1 and properties outlined in (P2). As for p , either (1.4) or (1.5) is used. For the capillary pressures and the fractional flow function, following set of properties is assumed, see Figure 1. They are consistent with experimental observations [3, 9]:

- (P1) The capillary pressures $p_c^{(j)} : (0, 1] \rightarrow [0, \infty)$, for $j = i, d$, are continuously differentiable and strictly decreasing in $(0, 1)$; $p_c^{(i)}(S) < p_c^{(d)}(S)$ for $S \in (0, 1)$ and $p_c^{(i)}(1) = p_c^{(d)}(1) = 0$ (no entry pressure).
- (P2) The fractional flow function $h : [0, 1] \rightarrow [0, \infty)$ is smooth with $h(0) = h(1) = 0$. There exists $S_M \in (0, 1)$ such that

$$h'(S) > 0 \text{ for } 0 < S < S_M, \text{ and } h'(S) < 0 \text{ for } S_M < S < 1.$$

Moreover, there exists inflection points $S_1, S_2 \in (0, 1)$ with $0 < S_1 < S_M < S_2 < 1$ such that

$$h''(S) > 0 \text{ for } \{0 < S < S_1\} \cup \{S_2 < S < 1\}, \text{ and } h''(S) < 0 \text{ for } S_1 < S < S_2.$$

The assumption (P1) is consistent with the van Genuchten model for capillary pressures. For h , the Brooks-Corey model (2.5) yields

$$h(S) = \frac{S^2(1-S)^2}{M^{-1}S^2 + (1-S)^2} \quad \text{with} \quad S_M = \frac{1}{(1+M^{-1/3})}. \quad (2.6)$$

3 Admissible shocks

In this section we consider shock solutions of equation (1.1) that originate from smooth solutions of (1.3). A shock is characterized by a constant left state S_l , a constant right state S_r , and a constant speed c . They are denoted by $\{S_l, S_r, c\}$ or

$$S(x, t) = \begin{cases} S_l & \text{for } x < ct, \\ S_r & \text{for } x > ct. \end{cases} \quad (3.1)$$

We call $\{S_l, S_r, c\}$ an admissible (i.e. vanishing capillarity) shock if it can be approximated, as $\delta \rightarrow 0$, by smooth solutions of (1.3) [14, 15]. To investigate this, we consider a special class of solutions of (1.3) in the form of travelling waves:

$$S_\delta(x, t) = \mathbf{S}(\eta), \quad p_\delta(x, t) = \mathbf{p}(\eta), \quad \text{with } \eta = \frac{x - ct}{\delta}. \quad (3.2)$$

Here $\mathbf{S} : \mathbb{R} \rightarrow [0, 1]$ is the saturation profile, $\mathbf{p} : \mathbb{R} \rightarrow [0, \infty]$ the capillary pressure profile and $c \in \mathbb{R}$ the wave-speed. We consider profiles that satisfy for the saturation

$$\lim_{\eta \rightarrow -\infty} \mathbf{S}(\eta) = S_l, \quad \lim_{\eta \rightarrow +\infty} \mathbf{S}(\eta) = S_r, \quad (3.3)$$

and for the pressure

$$\mathbf{p} \in L^\infty(\mathbb{R}) \quad (\text{bounded pressure}). \quad (3.4)$$

Clearly, if a smooth profile (3.2) exists and satisfies (3.3), then

$$S(x, t) = \lim_{\delta \rightarrow 0} S_\delta(x, t) = \lim_{\delta \rightarrow 0} \mathbf{S} \left(\frac{x - ct}{\delta} \right) = \begin{cases} S_l & \text{for } x < ct, \\ S_r & \text{for } x > ct. \end{cases}$$

Substituting (3.2) into (1.3) gives

$$-c\mathbf{S}' + [h(\mathbf{S})(1 + \mathbf{p}')] = 0 \text{ in } \mathbb{R}, \quad (3.5)$$

where primes denote differentiation. Integrating this expression yields

$$-c\mathbf{S} + h(\mathbf{S})(1 + \mathbf{p}') = A = \text{constant in } \mathbb{R}. \quad (3.6)$$

If \mathbf{S} satisfies (3.3), then (3.6) implies that \mathbf{p}' has a limit for $\eta \rightarrow \pm\infty$. The boundedness of pressure (3.4) then forces

$$\lim_{\eta \rightarrow -\infty} \mathbf{p}'(\eta) = \lim_{\eta \rightarrow +\infty} \mathbf{p}'(\eta) = 0. \quad (3.7)$$

Using this in (3.6) for $\eta = \pm\infty$ results in

$$-cS_l + h(S_l) = A, \quad (3.8a)$$

$$-cS_r + h(S_r) = A, \quad (3.8b)$$

giving

$$c = c(S_l, S_r) := \frac{h(S_l) - h(S_r)}{S_l - S_r} =: \frac{[[h]]}{[[S]]} \quad (\text{Rankine-Hugoniot}). \quad (3.9)$$

Substituting c and A in (3.6) yields

$$h(\mathbf{S}) \mathbf{p}' = (\mathbf{S} - S_l)[c(S_l, S_r) - c(S_l, \mathbf{S})], \quad \text{in } \mathbb{R}. \quad (3.10)$$

3.1 Equilibrium case: p given by (1.4)

Then $\mathbf{p} = p_c(\mathbf{S})$, and we write (3.10) as

$$D(\mathbf{S}) S' = F(\mathbf{S}) \text{ in } \mathbb{R}, \quad (3.11)$$

where

$$D(\mathbf{S}) = -h(\mathbf{S}) \frac{dp_c}{dS}(\mathbf{S}) > 0, \text{ and } F(\mathbf{S}) = (S_l - S)[c(S_l, S_r) - c(S_l, \mathbf{S})].$$

Clearly, $F(S_l) = F(S_r) = 0$.

If $S_l > S_r$, equation (3.11) has a solution satisfying (3.3) if $F(S) < 0$ for all $S_r < S < S_l$. Hence, the shock $\{S_l, S_r, c\}$ is admissible if c is given by (3.9) and

$$c(S_l, S_r) < c(S_l, S) \text{ for all } S_r < S < S_l. \quad (3.12a)$$

If $S_l < S_r$, the shock $\{S_l, S_r, c\}$ is admissible if (3.9) is satisfied, and

$$c(S_l, S_r) > c(S_l, S) \text{ for all } S_l < S < S_r. \quad (3.12b)$$

Conditions (3.12) are classical (Oleinik admissibility conditions), see [14, 15, 23]. To see which possible admissible shocks connect to the left or right states of the Riemann problem (1.1)–(1.2) we introduce two saturations. For $S_B < S_1$ (first inflection point of h), let $\bar{S}_B \in (S_B, 1)$ denote the unique point where the line through $(S_B, h(S_B))$ is tangent to the graph of h . If $S_B \geq S_1$, we set $\bar{S}_B = S_B$. A similar definition gives $\bar{S}_T \in (0, S_T)$, see Figure 3. Thus, the points \bar{S}_B and \bar{S}_T satisfy (in a limit sense if $S_B \geq S_1$ or $S_T \leq S_2$),

$$h'(\bar{S}_B) = \frac{h(\bar{S}_B) - h(S_B)}{\bar{S}_B - S_B} = c(S_B, \bar{S}_B), \quad h'(\bar{S}_T) = \frac{h(\bar{S}_T) - h(S_T)}{\bar{S}_T - S_T} = c(\bar{S}_T, S_T). \quad (3.13)$$

Applying (3.12) to Riemann problem (1.1)–(1.2), we note that if $S_B < S_1$, then S_B can serve as the right state $S_r = S_B$ of an admissible shock for left states between $S_B < S_l < \bar{S}_B$, see Figure 3. Similar for $S_l = S_T > S_2$ and $\bar{S}_T < S_r < S_T$.

3.2 Hysteretic case: p given by (1.5)

If $c(S_l, S_r) > 0$ or $c(S_l, S_r) < 0$, then any admissible shock in terms of (1.4) is also an admissible shock in terms of (1.5): To see this, fix $S_l > S_r$ and let (3.12) hold. Define the relation between $\mathbf{p}(\eta)$ and $\mathbf{S}(\eta)$ as

$$\mathbf{p}(\eta) = \begin{cases} p_c^{(i)}(\mathbf{S}(\eta)) & \text{if } c(S_l, S_r) > 0, \\ p_c^{(d)}(\mathbf{S}(\eta)) & \text{if } c(S_l, S_r) < 0. \end{cases}$$

Then, separately for $c(S_l, S_r) > 0$ and $c(S_l, S_r) < 0$, \mathbf{S} and \mathbf{p} are related through the classical relation (1.4) where p_c is replaced by $p_c^{(i)}$ and $p_c^{(d)}$ respectively. Consequently,

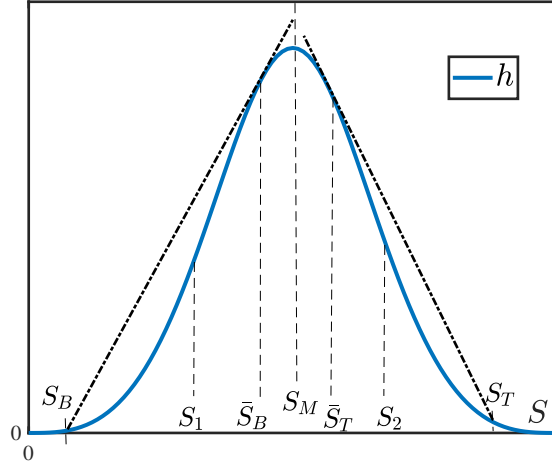


Figure 3: Graphical interpretation of conditions (3.12), applied to $S_B < S_1$ as the right state and $S_T > S_2$ as the left state. The saturations \bar{S}_B and \bar{S}_T are shown in the figure.

the existence of $\mathbf{S}(\eta)$ and $\mathbf{p}(\eta)$ solving (3.10) with boundary conditions (3.3)–(3.4) follows from Section 3.1. Observe that $\mathbf{S}'(\eta) < 0$ for all $\eta \in \mathbb{R}$ as a consequence of (3.11) and (3.12). Hence, recalling from (3.2) that $S_\delta(x, t) = \mathbf{S}(\eta)$ and $p_\delta(x, t) = \mathbf{p}(\eta)$, we have

$$\partial_t S_\delta(x, t) = -\frac{c(S_l, S_r)}{\delta} \mathbf{S}'(\eta) \begin{cases} > 0 & \text{when } c(S_l, S_r) > 0 \text{ (imbibition wave),} \\ < 0 & \text{when } c(S_l, S_r) < 0 \text{ (drainage wave).} \end{cases}$$

It is now straightforward to verify that (S_δ, p_δ) satisfies the hysteresis relation (1.5) for both $c(S_l, S_r) > 0$ and $c(S_l, S_r) < 0$. Hence, shocks that are admissible in terms of the equilibrium capillary pressure (1.4) are admissible in terms of the hysteretic capillary pressure (1.5) as well, provided $c \neq 0$. Note that the profiles (\mathbf{S}, \mathbf{p}) depend on the functional form of p_c , but not the resulting shock.

Observe that for $c(S_l, S_r) > 0$, the entire approximating wave (S_δ, p_δ) is in imbibition state since $p_\delta(x, t) = p_c^{(i)}(S_\delta(x, t))$ and $\partial_t S_\delta > 0$. Hence, we also refer to the resulting shock as being in **imbibition state**. Similarly, for $c(S_l, S_r) < 0$, the shock is in **drainage state** since $p_\delta(x, t) = p_c^{(d)}(S_\delta(x, t))$ and $\partial_t S_\delta < 0$. Effects of hysteresis are observed, if the hysteretic states ahead and behind the shock are different. This can only happen for stationary shocks having zero wave speed, i.e. $c(S_l, S_r) = 0$. For such shocks, Rankine-Hugoniot's expression (3.9) requires

$$c = c(S_l, S_r) = \frac{h(S_l) - h(S_r)}{S_l - S_r} = 0, \text{ implying } h(S_l) = h(S_r). \quad (3.14)$$

Note that this implies

$$S_r < S_M < S_l, \quad (\text{if } S_l > S_r). \quad (3.15)$$

Without a loss of generality we put the stationary shock at $x = 0$.

3.2.1 Case A: Connection between imbibition and drainage states

Let us first consider the case

$$S(0^-, t) = S_l \text{ is in drainage state,} \quad (3.16a)$$

$$S(0^+, t) = S_r \text{ is in imbibition state.} \quad (3.16b)$$

The case of S_l in imbibition and S_r in drainage is symmetrical. Here, the imbibition and drainage states are inherited from the approximating solutions as before.

For (3.16) to be an admissible stationary shock, (S_l, S_r) must be such that

(A1) Relation (3.14) is satisfied.

(A2) Equation (3.10), with $c(S_l, S_r) = 0$, has a solution $\mathbf{S}(\eta)$ satisfying (3.3).

(A3) The pressure profile $\mathbf{p} : \mathbb{R} \rightarrow \mathbb{R}$ satisfies

$$\mathbf{p}(\eta) = \begin{cases} p_c^{(d)}(\mathbf{S}(\eta)) & \text{when } \eta < 0, \\ p_c^{(i)}(\mathbf{S}(\eta)) & \text{when } \eta > 0. \end{cases} \quad (3.17)$$

Let $p_l := \mathbf{p}(-\infty)$ and $p_r := \mathbf{p}(+\infty)$. Then (3.17) implies

$$p_l = p_c^{(d)}(S_l) \text{ and } p_r = p_c^{(i)}(S_r). \quad (3.18)$$

Putting $c(S_l, S_r) = 0$ in (3.10) gives

$$h(\mathbf{S})\mathbf{p}' = h(S_l) - h(\mathbf{S}) = h(S_r) - h(\mathbf{S}) \quad \text{in } \mathbb{R}. \quad (3.19)$$

This equation implies that

$$\mathbf{p}' \text{ is bounded in } \mathbb{R}, \text{ and thus, } \mathbf{p} \text{ is continuous in } \mathbb{R}. \quad (3.20)$$

In particular, $\mathbf{p}(0^-) = \mathbf{p}(0^+)$, or from (3.17)

$$p_c^{(d)}(\mathbf{S}(0^-)) = p_c^{(i)}(\mathbf{S}(0^+)). \quad (3.21)$$

Combining (3.17) and (3.19) gives the problem

$$D^d(\mathbf{S}) \mathbf{S}' = h(\mathbf{S}) - h(S_l) \quad \text{in } \eta < 0, \quad (3.22a)$$

$$\mathbf{S}(-\infty) = S_l, \quad (3.22b)$$

where $D^d(\mathbf{S}) = -h(\mathbf{S})\frac{dp_c^{(d)}}{dS}(\mathbf{S}) > 0$. The unique solution of (3.22) is $\mathbf{S}(\eta) = S_l$ for all $\eta < 0$. This follows from the fact that if $S_l > S_r$, then $S_l > S_M$ from (3.15) and hence $h(\mathbf{S}(\eta)) < h(S_l)$ when $\mathbf{S}(\eta) > S_l$ and $h(\mathbf{S}(\eta)) > h(S_l)$ when $S_r < \mathbf{S}(\eta) < S_l$. Now suppose there exists $\eta_0 < 0$ such that $\mathbf{S}(\eta_0) > S_l$. Then $h(\mathbf{S}(\eta_0)) < h(S_l)$ implying $S'(\eta_0) < 0$. This means that $\mathbf{S}(\eta) > \mathbf{S}(\eta_0) > S_l$ for all $\eta < \eta_0$ contradicting $\mathbf{S}(-\infty) = S_l$. Similarly, if $S_r < \mathbf{S}(\eta_0) < S_l$ then $S'(\eta_0) > 0$, yielding a contradiction as well.

Repeating this reasoning for $\eta > 0$, we conclude that the unique solution of (A1)–(A3) is

$$(\mathbf{S}(\eta), \mathbf{p}(\eta)) = \begin{cases} (S_l, p_l) = (S_l, p_c^{(d)}(S_l)) & \text{for } \eta < 0, \\ (S_r, p_r) = (S_r, p_c^{(i)}(S_r)) & \text{for } \eta > 0, \end{cases} \quad (3.23)$$

where the pair (S_l, S_r) in addition to satisfying (3.14), also must satisfy $p_l = p_c^{(d)}(S_l) = p_c^{(i)}(S_r) = p_r$ due to (3.21), i.e.,

$$\llbracket h \rrbracket = h(S_r) - h(S_l) = 0, \quad \llbracket \mathbf{p} \rrbracket := p_r - p_l = 0. \quad (3.24)$$

We show that based on the assumptions (P1)–(P2), a unique pair $(S_l, S_r) = (S^*, S_*)$ with $0 < S_* \leq S_M \leq S^* < 1$ exists that satisfies (3.24). To see this, define the function $\hat{S} : [0, S_M] \rightarrow [S_M, 1]$ as

$$h(\hat{S}(S)) = h(S). \quad (3.25)$$

From (P2), the function $\hat{S}(\cdot)$ is decreasing, continuous, $\hat{S}(0) = 1$ and $\hat{S}(S_M) = S_M$, see also Figure 4 (left). Consider the strictly increasing function $p_c^{(d)}(\hat{S}(S))$ for $S \in (0, S_M)$. For $S = 0$, we have $p_c^{(d)}(\hat{S}(0)) = p_c^{(d)}(1) = p_c^{(i)}(1)$. Since $p_c^{(i)}$ is a strictly decreasing function, for $S > 0$ small enough one has $p_c^{(d)}(\hat{S}(S)) < p_c^{(i)}(S)$. On the other hand, $p_c^{(d)}(\hat{S}(S_M)) = p_c^{(d)}(S_M) > p_c^{(i)}(S_M)$. Thus, by intermediate value theorem, there exists $S_* \in (0, S_M)$ such that $p_c^{(d)}(\hat{S}(S_*)) = p_c^{(i)}(S_*)$, see Figure 4 (right). Thus, we put $S^* := \hat{S}(S_*)$.

Hence, shocks $\{S_l, S_r, 0\}$ (i.e. $c(S_l, S_r) = 0$), with their end states being in imbibition and drainage, are admissible if and only if (3.24) is satisfied with

$$S_l = S^*, \quad S_r = S_*, \quad p_l = p_c^{(d)}(S^*), \quad p_r = p_c^{(i)}(S_*) \quad (\text{Right state imbibition–left state drainage}), \quad (3.26a)$$

$$S_l = S_*, \quad S_r = S^*, \quad p_l = p_c^{(i)}(S_*), \quad p_r = p_c^{(d)}(S^*) \quad (\text{Left state imbibition–right state drainage}), \quad (3.26b)$$

where (S_*, S^*) with $0 < S_* \leq S_M \leq S^* < 1$ is the unique solution of

$$h(S_*) = h(S^*), \quad p_c^{(i)}(S_*) = p_c^{(d)}(S^*). \quad (3.27)$$

Connecting an imbibition state with another imbibition state demands that (3.24) be satisfied with $p_l = p_c^{(i)}(S_l)$ and $p_r = p_c^{(i)}(S_r)$ which has the unique solution $S_l = S_r$. The same result holds for connecting a drainage state with another drainage state. Hence, no non-trivial stationary shock ($S_l \neq S_r$) exists in these cases.

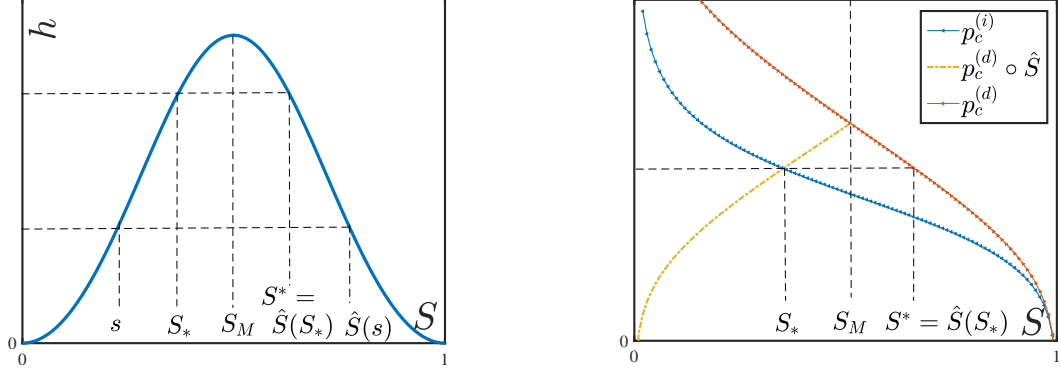


Figure 4: Construction of the pair (S_*, S^*) defined in (3.27). (left) The function $\hat{S}(\cdot)$ in the h - S diagram. (right) The composite function $p_c^{(d)} \circ \hat{S}$ and its intersection with $p_c^{(i)}$.

3.2.2 Case B: One state undetermined

It is also possible that one of the states (S_l, S_r) is undetermined (neither in imbibition nor in drainage). To demonstrate the admissibility for this case, we first assume that the left state is undetermined and the right state is in imbibition. Using $\partial_t S = -\frac{c(S_l, S_r)}{\delta} S' = 0$ in (1.5), we have that $\{S_l, S_r, 0\}$ is an admissible stationary shock if

(B1) Relation (3.14) is satisfied.

(B2) Equation (3.10), with $c(S_l, S_r) = 0$, has a solution $\mathbf{S}(\eta)$ satisfying (3.3).

(B3) The pressure profile $\mathbf{p} : \mathbb{R} \rightarrow \mathbb{R}$ satisfies

$$\mathbf{p}(\eta) \begin{cases} \in [p_c^{(i)}(\mathbf{S}(\eta)), p_c^{(d)}(\mathbf{S}(\eta))] & \text{when } \eta < 0, \\ = p_c^{(i)}(\mathbf{S}(\eta)) & \text{when } \eta > 0. \end{cases} \quad (3.28)$$

Following the same arguments as before, we have

$$\mathbf{p}(0^-) = \mathbf{p}(0^+), \quad (3.29)$$

$$(\mathbf{S}(\eta), \mathbf{p}(\eta)) = (S_r, p_r) = (S_r, p_c^{(i)}(S_r)) \text{ for all } \eta > 0. \quad (3.30)$$

What remains is the $\eta < 0$ problem which reads

$$\left. \begin{aligned} h(\mathbf{S})\mathbf{p}' &= h(S_l) - h(\mathbf{S}) \\ p_c^{(i)}(\mathbf{S}) &\leq \mathbf{p} \leq p_c^{(d)}(\mathbf{S}) \end{aligned} \right\} \text{ for all } \eta < 0, \quad (3.31a)$$

$$S(-\infty) = S_l, \quad \mathbf{p}(0^-) = p_r. \quad (3.31b)$$

There exists infinitely many solutions of (3.31). However, in purview of the time-dependent problem (1.3),(1.5) one gets in this case $\partial_t S_\delta(x, t) = -\frac{c(S_l, S_r)}{\delta} \mathbf{S}'(\eta) = 0$ for all $t > 0$. Since the initial condition (1.2) is constant for $x < 0$, the physically relevant solution is the constant state solution $\mathbf{S} = S_l$, yielding $\mathbf{p} = p_l$. This satisfies (B1)–(B3) provided,

$$[[h]] = h(S_r) - h(S_l) = 0, \quad [[\mathbf{p}]] = p_r - p_l = 0, \quad (3.32a)$$

$$p_c^{(i)}(S_l) < p_l = p_r = p_c^{(i)}(S_r) \leq p_c^{(d)}(S_l). \quad (3.32b)$$

Hence, also in this case, condition (3.24) is satisfied. We show below that additionally (3.32b) is satisfied if and only if

$$S_r \in [S_*, S_M] \text{ and } S_l = \hat{S}(S_r) \in [S_M, S^*], \quad (3.33)$$

where (S_*, S^*) and the function $\hat{S}(\cdot)$ are defined in (3.27) and (3.25) respectively. Indeed, from the definition of $\hat{S}(\cdot)$, if $S_r \in (S_*, S_M)$ then $h(S_l) = h(\hat{S}(S_r)) = h(S_r)$ and $S_l \in (S_M, S^*)$. From (P1) it directly follows that, $p_c^{(i)}(S_l) < p_c^{(i)}(S_r) = p_r$. To get $p_c^{(i)}(S_r) \leq p_c^{(d)}(S_l)$ we consider the strictly increasing function $p_\Delta(S) := p_c^{(d)}(\hat{S}(S)) - p_c^{(i)}(S)$ for $S \in (0, S_M)$, see the properties of $\hat{S}(\cdot)$, (P1) and Figures 4 and 5 (right). The function has a zero at $S = S_*$. This means $p_\Delta(S_r) \geq 0$, or $p_c^{(d)}(S_l) = p_c^{(d)}(\hat{S}(S_r)) \geq p_c^{(i)}(S_r)$. The construction is also shown in Figure 5. It is straightforward to verify that if $S_r < S_*$ then (3.32) can not be satisfied, leaving (3.33) as the only possibility to satisfy (3.32).

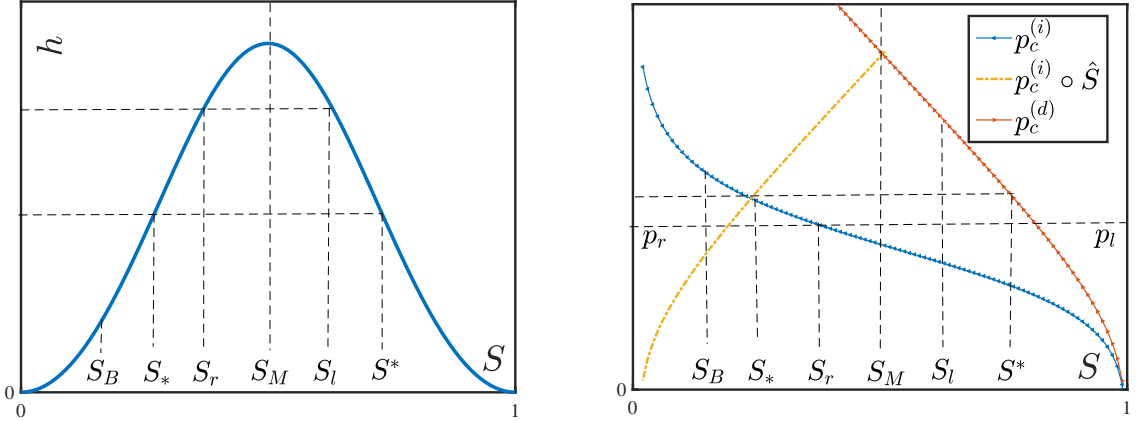


Figure 5: The saturations S_l , S_r , S_* and S^* in the h - S plane (left), and p_c - S plane (right). The pressure $p_l = p_r = p_c^{(i)}(S_r) \in [p_c^{(i)}(S_l), p_c^{(d)}(S_l)]$ is also shown.

Condition (3.33) serves as the admissibility criterion when the left state is undetermined and the right state is in imbibition. Considering all combinations, including undetermined-drainage, imbibition-undetermined, drainage-undetermined and undetermined-undetermined, the complete list of admissible stationary shocks $\{S_l, S_r, 0\}$ with $S_l \neq S_r$ is given in Table 1.

Left state	Right state	S_l	S_r	p_l	p_r
drainage	imbibition	$= S^*$	$= S_*$	$= p_c^{(d)}(S_l)$	$= p_c^{(i)}(S_r)$
imbibition	drainage	$= S_*$	$= S^*$	$= p_c^{(i)}(S_l)$	$= p_c^{(d)}(S_r)$
undetermined	imbibition	$\in [S_M, S^*]$	$\in [S_*, S_M]$	$\in (p_c^{(i)}(S_l), p_c^{(d)}(S_l)]$	$= p_c^{(i)}(S_r)$
imbibition	undetermined	$\in [S_*, S_M]$	$\in [S_M, S^*]$	$= p_c^{(i)}(S_l)$	$\in (p_c^{(i)}(S_r), p_c^{(d)}(S_r)]$
undetermined	drainage	$\in [S_*, S_M]$	$\in [S_M, S^*]$	$\in [p_c^{(i)}(S_l), p_c^{(d)}(S_l)]$	$= p_c^{(d)}(S_r)$
drainage	undetermined	$\in [S_M, S^*]$	$\in [S_*, S_M]$	$= p_c^{(d)}(S_l)$	$\in [p_c^{(i)}(S_r), p_c^{(d)}(S_r)]$
undetermined	undetermined	$\in [S_*, S^*]$	$\in [S_*, S^*]$	$\in [p_c^{(i)}(S_l), p_c^{(d)}(S_l)]$	$\in [p_c^{(i)}(S_r), p_c^{(d)}(S_r)]$

Table 1: All admissible stationary shocks $\{S_l, S_r, 0\}$ with $S_l \neq S_r$. They satisfy the condition $[[h]] = h(S_r) - h(S_l) = 0$, and $[[p]] = p_r - p_l = 0$ where S_l , S_r , p_l and p_r are given in the table. The states on the left and the right of the shocks are also stated. Imbibition state corresponds to $p_c^{(i)}$ curve being used to relate S_l and p_l or S_r and p_r . Similarly, drainage state corresponds to the use of $p_c^{(d)}$. Undetermined left state implies that $p_l \in [p_c^{(i)}(S_l), p_c^{(d)}(S_l)]$ and undetermined right state implies $p_r \in [p_c^{(i)}(S_r), p_c^{(d)}(S_r)]$.

Remark 3.1 (Non-uniqueness of the pair (S_l, S_r)). *Note that (3.33) does not yield a unique pair (S_l, S_r) , but rather an interval of possibilities. This is due to the fact that the pressure in the underlying hysteresis model is not prescribed in one (or both) states where it satisfies the inclusion part of (1.5).*

4 Vanishing capillarity solutions of the Buckley-Leverett equation

We construct the solution of the Riemann problem (1.1)–(1.2) with the admissibility conditions from Section 3. A solution of (1.1) is composed of constant states separated by shocks and rarefaction waves. We recall that a rarefaction wave is a smooth solution of (1.1) having the form

$$S(x, t) = r(\zeta) \text{ where } \zeta = x/t. \quad (4.1)$$

Then for $r(\cdot)$ results the equation

$$\frac{dh}{dS}(r(\zeta)) = \zeta \text{ for } \zeta_l < \zeta < \zeta_r, \quad (4.2)$$

where

$$r(\zeta_l) = S_l, \text{ and } r(\zeta_r) = S_r \quad \text{or} \quad \zeta_l = \frac{dh}{dS}(S_l), \text{ and } \zeta_r = \frac{dh}{dS}(S_r).$$

Rarefaction waves are well-defined if

$$f''(S) \text{ does not change sign for all } \min\{S_l, S_r\} \leq S \leq \max\{S_l, S_r\}. \quad (4.3)$$

We show below how to construct solutions of (1.1) with rarefaction waves satisfying (4.2) along with condition (4.3), and shocks satisfying the admissibility conditions from Section 3. For completeness, we briefly recall the classical Buckley-Leverett construction.

4.1 Classical construction

The construction of vanishing capillarity solutions for the classical case is well established, see [14, 23]. Recalling the definitions of \bar{S}_B and \bar{S}_T in (3.13), we identify three cases.

Case I: $S_T \leq S_M$:

In this case $S_B < S_M$ since $S_B < S_T$. The vanishing capillarity solutions are

$$\underline{\text{If } S_T \leq \bar{S}_B}: \quad S(x, t) = \begin{cases} S_T & \text{for } x < c(S_B, S_T) t, \\ S_B & \text{for } x > c(S_B, S_T) t, \end{cases} \quad (4.4a)$$

and with $r(\cdot)$ defined in (4.2),

$$\underline{\text{If } S_T > \bar{S}_B}: \quad S(x, t) = \begin{cases} S_T & \text{for } x < h'(S_T) t, \\ r(x/t) & \text{for } h'(S_T) t < x < c(S_B, \bar{S}_B) t, \\ S_B & \text{for } x > c(S_B, \bar{S}_B) t. \end{cases} \quad (4.4b)$$

These expressions represent a monotonically decreasing profile that moves to the right, describing an imbibition state. Hence $S(0^-, t) = S(0^+, t) = S_T$ for all $t > 0$.

Case II: $S_B \geq S_M$:

In this case $S_T > S_M$. The vanishing capillarity solutions are

$$\underline{\text{If } S_B \geq \bar{S}_T}: \quad S(x, t) = \begin{cases} S_T & \text{for } x < c(S_B, S_T) t, \\ S_B & \text{for } x > c(S_B, S_T) t; \end{cases} \quad (4.5a)$$

and

$$\underline{\text{If } S_B < \bar{S}_T}: \quad S(x, t) = \begin{cases} S_T & \text{for } x < c(\bar{S}_T, S_T) t, \\ r(x/t) & \text{for } h'(S_B) t > x > c(\bar{S}_T, S_T) t, \\ S_B & \text{for } x > h'(S_B) t. \end{cases} \quad (4.5b)$$

These expressions represent a monotonically decreasing profile that moves to the left, describing an drainage state. Hence $S(0^-, t) = S(0^+, t) = S_B$ for all $t > 0$.

Case III: $S_B < S_M < S_T$:

In this case we have (recall the definition of (3.13)),

$$S(x, t) = \begin{cases} S_T & \text{for } x < c(\bar{S}_T, S_T)t < 0, \\ r(x/t) & \text{for } c(\bar{S}_T, S_T)t < x < c(S_B, \bar{S}_B)t, \\ S_B & \text{for } 0 < c(S_B, \bar{S}_B)t < x. \end{cases} \quad (4.6)$$

4.2 Construction with capillary hysteresis

Vanishing capillarity solution for Case I and II: Observe that in Case I of Section 4.1 ($S_T < S_M$) the shock is in an imbibition state and the rarefaction wave part, if it exists, satisfies $\partial_t S > 0$. Hence, the vanishing capillarity solution as a whole is in imbibition state. Similarly, for Case II the entire solution is in drainage state. Consequently, based on the discussions in Section 3.2 and the fact that the classical solution does not depend on the specific form of p_c , the vanishing capillarity solutions for the capillary hysteresis model in Case I and Case II are identical to the classical ones.

Vanishing capillarity solution for Case III: As in the classical case, we construct a solution which is in imbibition state when $x > 0$ and drainage state when $x < 0$. Hence one expects to have a stationary shock at $x = 0$. We restrict ourselves to the case

$$0 < S_B < S_M < S_T < 1, \quad \text{and} \quad h(S_B) \leq h(S_T), \quad (4.7)$$

the solution for $h(S_T) \leq h(S_B)$ being symmetrical. With respect to the cases A and B in Section 3.2 we divide the discussion in two parts.

4.2.1 Case $S_T \geq S^* \geq S_M$

The restriction (4.7) implies that $S_B \leq S_*$. Recalling from Table 1, any stationary shock at $x = 0$ must satisfy

$$\lim_{x \searrow 0} S(x, t) = S_r \in [S_*, S_M] \quad \text{and} \quad \lim_{x \nearrow 0} S(x, t) = S_l = \hat{S}(S_r) \in [S_M, S^*],$$

where the function $\hat{S}(\cdot)$ and $\{S_*, S^*\}$ are defined in (3.25) and (3.27) respectively.

Now suppose $S_r \in (S_*, S_M]$. Then we are in the situation of Figure 5 (left). The part connecting S_B to S_r describes an imbibition profile in $\{(x, t) : x > 0, t > 0\}$: see Case I with S_T replaced by S_r . Similarly, in $\{(x, t) : x < 0, t > 0\}$ we have a drainage profile: see Case II with S_B replaced by S_l . However, again using Table 1, the left state in drainage and the right state in imbibition implies $S_r = S_*$. Hence, $S_r > S_*$ yields a contradiction and we are left with $S_r = S_*$ and $S_l = S^*$ as the unique possibility.

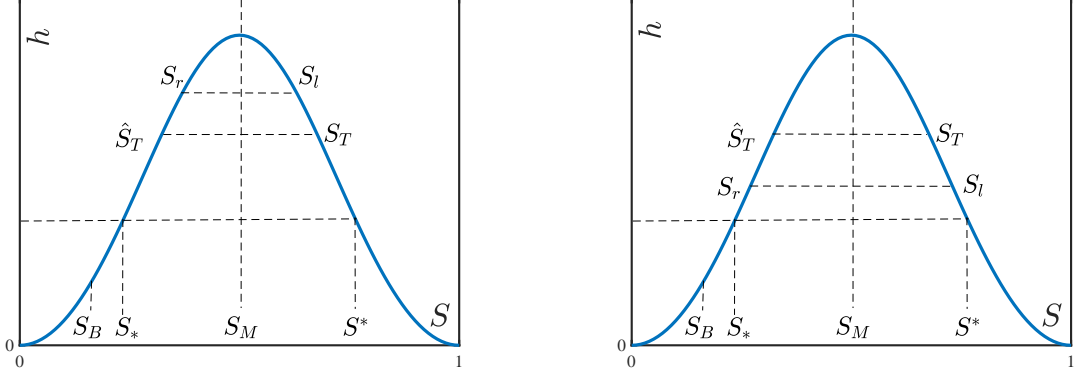


Figure 6: Graph of h with possible constructions: (i) $S_M \leq S_l < S_T$ (left), and (ii) $S_T < S_l \leq S^*$ (right).

Vanishing capillarity solution: For $x > 0$ and $t > 0$,

$$S(x, t) \text{ is given by (4.4) where } S_T = S_*. \quad (4.8a)$$

For $x < 0$ and $t > 0$,

$$S(x, t) \text{ is given by (4.5) where } S_B = S^*. \quad (4.8b)$$

Remark 4.1 (Convergence of (4.8) to the classical case). *In the absence of hysteresis, $p_c(S) = p_c^{(i)}(S) = p_c^{(d)}(S)$. This means that for the standard model, $S_* = S^* = S_M$. Hence, saturation becomes continuous at $x = 0$ and the vanishing capillarity solution (4.8) becomes identical to (4.6).*

4.2.2 Case $S^* > S_T > S_M$

Let $\check{S}_T \in (S_*, S_M]$ be such that $\hat{S}(\check{S}_T) = S_T$, or in other words

$$\check{S}_T = \hat{S}^{-1}(S_T) \in (S_*, S_M) \text{ for all } S_T \in (S_M, S^*). \quad (4.9)$$

Then, restriction (4.7) implies that $S_B < \check{S}_T$, see also Figure 6.

(i) $S_M \leq S_l < S_T$: This would give a drainage wave connecting S_T and S_l in $\{(x, t) : x < 0, t > 0\}$ and an imbibition wave connecting S_r and S_B in $\{(x, t) : x > 0, t > 0\}$. This contradicts Table 1 since this would yield $S_r = S_*$ and $S_l = S^*$.

(ii) $S_T < S_l \leq S^*$: This would result in an imbibition wave connecting S_T and S_l in $\{(x, t) : x < 0, t > 0\}$. This contradicts again Table 1 since it would imply that $S_l \in [S_*, S_M]$.

Hence, we are left with

Vanishing capillarity solution: for $x > 0$ and $t > 0$,

$$S(x, t) \text{ is given by (4.4) where } S_T = \check{S}_T. \quad (4.10a)$$

For $x < 0$ and $t > 0$,

$$S(x, t) = S_T \quad (\text{solution is frozen}). \quad (4.10b)$$

The vanishing capillarity solutions for the cases $S_T > S_*$ and $S_T \in (S_M, S^*)$ are shown in Figure 7. Observe that there is no classical counterpart of (4.10). The solution plotted in Figure 2 (right) for the play-type hysteresis model is of this type.

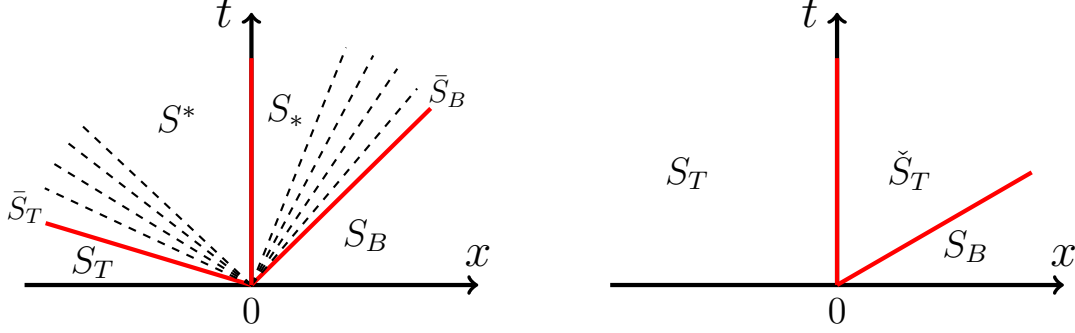


Figure 7: Vanishing capillarity solutions for the case (left) $S_T > S^*$ with the specific ordering $S_B < S_1 < \bar{S}_B < S_* < S^* < \bar{S}_T < S_2 < S_T$, and for the case (right) $S_M < S_T < S^*$ with the ordering $S_B < \check{S}_T < \bar{S}_B < S_M < S_T < S^*$. The red lines represent shocks and the dashed regions are the rarefaction waves. In the left figure, there are two traveling shocks $S_B-\bar{S}_B$ and $S_T-\bar{S}_T$ and a stationary shock S_*-S^* . In the right figure, there is one shock $S_B-\check{S}_T$ and a stationary shock \check{S}_T-S_T . The S profiles for these two cases were shown in Figure 2 and will be discussed again in Section 5.

Remark 4.2 (Weak solutions of (1.1)). *It is straightforward to check that solutions (4.8)–(4.10) are weak solutions of (1.1)–(1.2) in the usual sense: i.e., they satisfy*

$$\int_0^\infty \int_{\mathbb{R}} [S \partial_t \varphi + h(S) \partial_x \varphi] dx dt + S_T \int_{\mathbb{R}^-} \varphi(x, 0) dx + S_B \int_{\mathbb{R}^+} \varphi(x, 0) dx = 0, \quad (4.11)$$

for all $\varphi \in C^1(\mathbb{R} \times \mathbb{R}^+)$ vanishing for large t and $|x|$. This is evident from the fact that the Rankine-Hugoniot condition is satisfied for all the admissible shocks. The specific criteria developed in Section 3 select the physically relevant solution among those satisfying (4.11).

Remark 4.3 (Generality of the results with respect to other hysteresis models). *The admissible shocks presented in Table 1 and the vanishing capillarity solutions presented in*

(4.8) and (4.10) are consistent with any hysteresis model that satisfies the condition

$$p \in \mathcal{H}, \text{ and } p = \begin{cases} p_c^{(i)}(S) & \text{implies } \partial_t S \geq 0, \\ \in [p_c^{(i)}(S), p_c^{(d)}(S)] & \text{allows } \partial_t S = 0, \\ p_c^{(d)}(S) & \text{implies } \partial_t S \leq 0. \end{cases} \quad (4.12)$$

Most of the commonly used hysteresis models, including the Lenhard-Parker model [24] and the extended play-type model [8] belong to this category. The results are consistent with any model satisfying (4.12) since the models only differ in the description of (S, p) when $p \in (p_c^{(i)}(S), p_c^{(d)}(S))$, i.e. when the hysteretic state is undetermined. As a result, if a stationary shock connects imbibition to drainage, then the set of equations (A1)–(A3) are valid also for a model satisfying (4.12). Thus, the resulting shocks are unaltered. Similarly, (B1)–(B3) (in particular (B3)) are consistent with describing the shock when one of the states is undetermined since in this case $\partial_t S = -\frac{c(S_l, S_r)}{\delta} S' = 0$ which is allowed by (4.12). Hence, models satisfying (4.12) are consistent with admissible shocks listed in Table 1, and consequently with the vanishing capillarity solutions obtained in this section.

5 Numerical Results

To solve (1.2), (1.5) numerically, (1.5) is usually regularised in the following way:

$$p = \begin{cases} p_c^{(i)}(S) - \tau \partial_t S & \text{when } \partial_t S > 0, \\ \in [p_c^{(i)}(S), p_c^{(d)}(S)] & \text{when } \partial_t S = 0, \\ p_c^{(d)}(S) - \tau \partial_t S & \text{when } \partial_t S < 0. \end{cases} \quad (5.1)$$

The relaxation parameter $\tau > 0$ (dynamic capillarity coefficient) was mentioned briefly in Section 1. The parameter τ is kept small to approximate the results of the model (1.5) accurately. This also ensures that τ does not exceed the threshold required to cause effects such as saturation overshoot [19, 21].

We solve (1.3) and (5.1) in a domain $(-L, L)$ for a large $L > 0$. The boundary conditions used are

$$h(S)[1 + \delta \partial_x p](-L, t) = h(S_T), \text{ and } p(L, t) = p_c^{(i)}(S_B) \text{ for all } t > 0. \quad (5.2)$$

The approach for solving the system (1.3), (5.1)–(5.2), is based on rearranging (5.1) to express $\partial_t S$ as a function of S and p , and using this, to consider (1.3) as an elliptic equation for the pressure. Details of the numerical method are given in Section 5 of [19], see also the numerical sections of [21, 34]. Cell centered finite difference method with a uniform mesh is used for the computation with Δx and Δt representing the mesh and the time step sizes respectively. The following choices of parameters are made

$$\tau = 0.01, \delta = 0.25, L = 100, \Delta x = 0.01, \Delta t = 0.0001.$$

These values ensure both that our parabolic solver is converging and the capillarity solutions are sufficiently close to their hyperbolic limit. Since smaller δ also implies that the profiles take longer to develop, we have optimized the value of δ so that a good approximation of the developed profile is obtained in a reasonable time. Figure 8 shows that the choice of τ gives a good approximation to the limiting case $\tau \rightarrow 0$. Decreasing τ further significantly increases the number of linear iterations required.

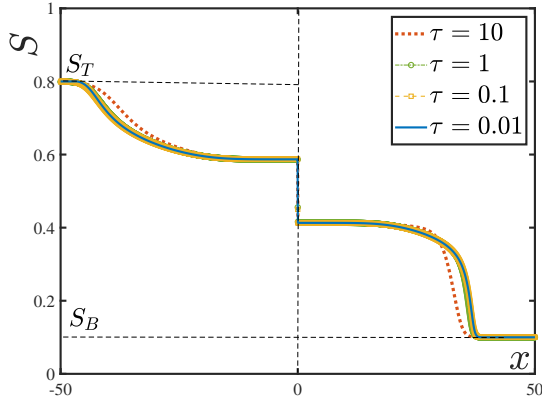


Figure 8: Saturation profiles for different τ values in (5.1) with reference to the numerical experiment conducted in Figure 9. Here, $t = 100$. The profiles converge to a limiting profile for $\tau \rightarrow 0$ and are practically indistinguishable for $\tau < 1$.

5.1 Validation

For validating our predictions of Section 4 we use Brooks-Corey expression (2.6) for h with $M = 1$. This gives $S_M = 0.5$. Van Genuchten parametrization is used here to model the capillary curves. Two choices for the imbibition and drainage curves are made. At first, we take $p_c^{(i)}(\cdot)$ and $p_c^{(d)}(\cdot)$ close to each other, i.e.,

$$p_c^{(i)}(S) = 3.5 (S^{-\frac{1}{q_1}} - 1)^{1-q_1} \text{ with } q_1 = 0.92, \text{ and } p_c^{(d)}(S) = p_c^{(i)}(S) + \frac{1}{2}(1 - S),$$

see Figure 9 (right). In this case, direct computation shows that $S_* = 0.4121$ and $S^* = 0.5879$. We take $S_T = 0.8$ and $S_B = 0.1$ implying that $S_T > S^*$. The vanishing capillarity solution in this scenario is (4.8). It consists of shocks between $S_T - \bar{S}_T$ and $S_B - \bar{S}_B$, rarefaction waves between $\bar{S}_T - S^*$ and $\bar{S}_B - S_*$ and a stationary shock from S_* to S^* at $x = 0$, see Figure 2 (left) and Figure 9 (left). The numerically computed solution is shown in Figure 9 (left) and in the p_c - S plane in Figure 9 (right). The numerically obtained capillary solutions are close to the predicted vanishing capillarity solutions. The

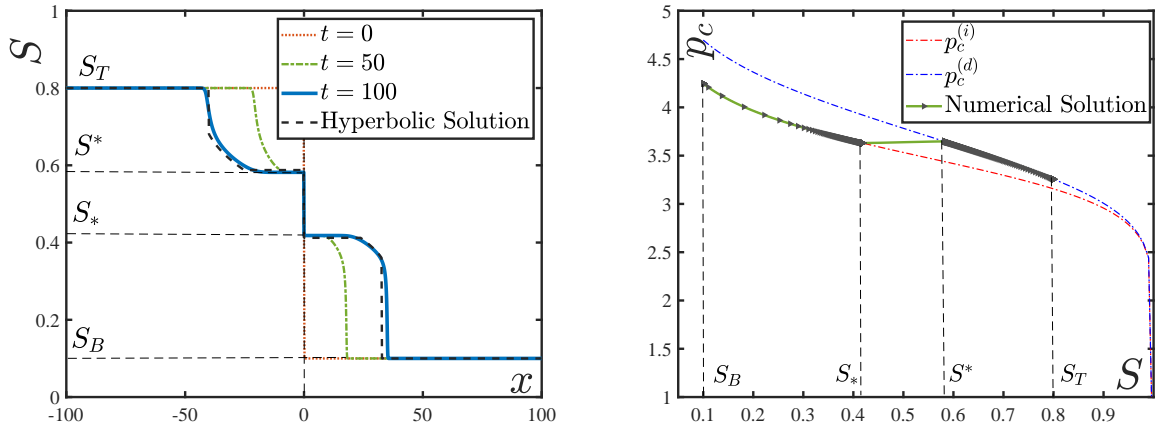


Figure 9: (left) Numerically computed capillarity solution against the vanishing capillarity solution (black dashed line) for $S_T > S^*$ given by (4.8). Here, $\delta = 0.25$, $S_B = 0.1$ and $S_T = 0.8$. The numerical solution is shown at $t = 50$ and $t = 100$. (right) The same numerical solution in the p_c - S plane at $t = 100$. For $x > 0$, the solution is on top of $p_c^{(i)}$ (imbibition state), whereas, for $x < 0$ it is on top of $p_c^{(d)}$ (drainage state). A horizontal shift is observed at $x = 0$ implying that the pressure is continuous across $x = 0$, see (3.24).

minor differences are due to $\delta > 0$, $\tau > 0$ and numerical errors. Note that the counter-current flow for $x < 0$ stems from non-monotonicity of h , since the flux at $x = 0$ is $h(S_*)$ which is greater than the flux at the left boundary.

Next, we take $p_c^{(i)}$ same as before but $p_c^{(d)}$ as in Figure 1 (right):

$$p_c^{(d)}(S) = 5(S^{-\frac{1}{q_2}} - 1)^{1-q_2} \text{ with } q_2 = 0.9.$$

These curves resemble experimentally obtained retention curves (see [22]) and were taken from [19]. With (S_B, S_T) same as before, one has $S_T < S^* = 0.8759$ in this case. Hence, recalling Section 4.2.2, particularly (4.10), the solution is frozen for $x < 0$. For $x > 0$, there is a shock connecting $\check{S}_T = 0.2$ and S_B . This behaviour is mimicked by the computed capillarity solutions, see Figure 10. In this case, the total mass is still balanced since the total rate of water infiltration is $c(S_B, \check{S}_T)(\check{S}_T - S_B) = h(\check{S}_T) - h(S_B) = h(S_T) - h(S_B)$, which is precisely equal to the difference of fluxes at the left and the right boundaries.

6 Conclusion

In this paper we considered the Buckley-Leverett equation (1.1) with non-monotone flux function. This occurs in gravity driven flows. In the presence of hysteresis, such as (1.5),

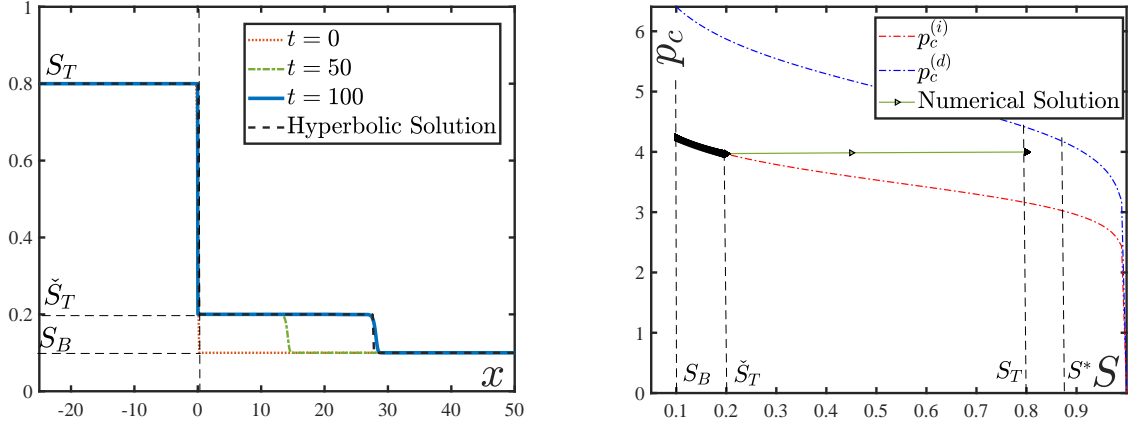


Figure 10: (left) Computed capillarity solution against the vanishing capillarity solution (black dashed line) for $S_M < S_T < S^*$ given by (4.10). Here, $\delta = 0.25$, $S_B = 0.1$ and $S_T = 0.8$. The saturation for $x < 0$ does not change and $S(0, t) \approx \check{S}_T = 0.2$ for all $t > 0$. (right) The numerical solution in the p_c - S plane for $t = 100$. The pressure at $x = 0$ is approximately $p_l = p_c^{(i)}(\check{S}_T)$.

the hyperbolic (vanishing capillarity) limit of solutions to (1.3) differs from the classical solutions obtained through the equilibrium expression (1.4). In particular, a solution to the Riemann problem (1.1)–(1.2) has a stationary shock at $x = 0$ if the left ($x < 0$) and the right ($x > 0$) states lie in the increasing and decreasing parts of the flux function respectively, or vice versa. The hysteretic states on the left and right become different in this case and thus, different capillary relations are used. Using travelling wave solutions, an admissibility condition (3.24) is derived for the stationary shocks. The condition states that the flux function h and the pressure corresponding to the hysteretic state of the system, remain continuous across the shock. It is then used to derive all admissible shocks. They are listed in Table 1. The shocks are classified into two categories. The first (Case A) connects imbibition states to drainage states, and the second (Case B) has one of the states undetermined.

Depending on the values of the Riemann data with respect to characteristic points that are easily computable a-priori from h and the capillary curves, two possibilities are identified (corresponding to Case A and Case B) when the stationary shocks occur. The vanishing capillarity solutions for these cases are given by (4.8) and (4.10). Interestingly, the solution (4.10) remains frozen in time in one of the halves and thus, differs significantly from the classical solution. To our knowledge, this is a novel observation. The predictions were validated using numerical experiments.

Acknowledgment

K. Mitra acknowledges the support from Radboud University. Parts of the research for K. Mitra were also funded by INRIA Paris through the ERC Gatipor grant, TU Dortmund University, Shell–NWO CSER program (grant 14CSER016) and Hasselt University (grant BOF17BL04). C.J. van Duijn is supported by the Darcy Center of Eindhoven University of Technology and Utrecht University. The authors would like to thank Prof. Sorin Pop for many fruitful discussions on the topic.

References

- [1] E. Abreu and W. Lambert. Computational modeling technique for numerical simulation of immiscible two-phase flow problems involving flow and transport phenomena in porous media with hysteresis. In *AIP Conference Proceedings 4*, volume 1453, pages 141–146. American Institute of Physics, 2012.
- [2] B. Andreianov and C. Cancès. Vanishing capillarity solutions of Buckley–Leverett equation with gravity in two-rocks’ medium. *Computational Geosciences*, 17(3):551–572, 2013.
- [3] J. Bear. *Hydraulics of groundwater*. McGraw-Hill International Book Co., 1979.
- [4] P. Bedrikovetsky, D. Marchesin, and P.R. Ballin. Mathematical model for immiscible displacement honouring hysteresis. In *SPE Latin America/Caribbean Petroleum Engineering Conference*. Society of Petroleum Engineers, 1996.
- [5] E.E. Behi-Gornostaeva, K. Mitra, and B. Schweizer. Traveling wave solutions for the Richards equation with hysteresis. *IMA Journal of Applied Mathematics*, 84(4):797–812, 2019.
- [6] A.Y. Beliaev and S.M. Hassanizadeh. A theoretical model of hysteresis and dynamic effects in the capillary relation for two-phase flow in porous media. *Transport in Porous Media*, 43(3):487–510, 2001.
- [7] X. Cao and I.S. Pop. Two-phase porous media flows with dynamic capillary effects and hysteresis: Uniqueness of weak solutions. *Computers & Mathematics with Applications*, 69(7):688 – 695, 2015.
- [8] C.J. van Duijn and K. Mitra. Hysteresis and horizontal redistribution in porous media. *Transport in Porous Media*, 122(2):375–399, 2018.
- [9] R. Helmig. *Multiphase flow and transport processes in the subsurface: a contribution to the modeling of hydrosystems*. Springer-Verlag, 1997.
- [10] J. Koch, A. Rätz, and B. Schweizer. Two-phase flow equations with a dynamic capillary pressure. *European Journal of Applied Mathematics*, 24(1):49–75, 2013.
- [11] P. Krejci. *Hysteresis, convexity and dissipation in hyperbolic equations*. Tokyo: Gakkotosho, 1996.

- [12] A. Lamacz, A. Rätz, and B. Schweizer. A well-posed hysteresis model for flows in porous media and applications to fingering effects. *Advances in Mathematical Sciences and Applications*, 21(2):33, 2011.
- [13] P.D. Lax. *Hyperbolic systems of conservation laws and the mathematical theory of shock waves*. Society for Industrial and Applied Mathematics, 1973.
- [14] P.G. LeFloch. *Hyperbolic systems of conservation laws: the theory of classical and nonclassical shock waves*. Springer Science & Business Media, 2002.
- [15] T.P. Liu. *Hyperbolic and viscous conservation laws*. Society for Industrial and Applied Mathematics, 2000.
- [16] C.T. Miller, K. Bruning, C.L. Talbot, J.E. McClure, and W.G. Gray. Nonhysteretic capillary pressure in two-fluid porous medium systems: Definition, evaluation, validation, and dynamics. *Water Resources Research*, 55(8):6825–6849, 2019.
- [17] K. Mitra. *Mathematical complexities in porous media flow*. PhD thesis, Eindhoven University of Technology & Hasselt University, 2019. ISBN: 978-90-386-4845-3.
- [18] K. Mitra. Existence and properties of solutions of the extended play-type hysteresis model. *Journal of Differential Equations*, 288:118–140, 2021.
- [19] K. Mitra, T. Köppl, I.S. Pop, C.J. van Duijn, and R. Helmig. Fronts in two-phase porous media flow problems: The effects of hysteresis and dynamic capillarity. *Studies in Applied Mathematics*, 144(4):449–492, 2020.
- [20] K. Mitra, A. Rätz, and B. Schweizer. Travelling wave solutions for gravity fingering in porous media flows. *arXiv preprint arXiv:2011.10792*, 2020.
- [21] K. Mitra and C.J. van Duijn. Wetting fronts in unsaturated porous media: The combined case of hysteresis and dynamic capillary pressure. *Nonlinear Analysis: Real World Applications*, 50:316 – 341, 2019.
- [22] N.R. Morrow and C.C. Harris. Capillary equilibrium in porous materials. *Society of Petroleum Engineers*, 5(01):15–24, 1965.
- [23] O.A. Oleinik. Discontinuous solutions of non-linear differential equations. *Uspekhi Matematicheskikh Nauk*, 12(3):3–73, 1957.
- [24] J.C. Parker, R.J. Lenhard, and T. Kuppusamy. A parametric model for constitutive properties governing multiphase flow in porous media. *Water Resources Research*, 23(4):618–624, 1987.
- [25] J.R. Philip. Horizontal redistribution with capillary hysteresis. *Water Resources Research*, 27:1459–1469, 1991.
- [26] B. Plohr, D. Marchesin, P. Bedrikovetsky, and P. Krause. Modeling hysteresis in porous media flow via relaxation. *Computational Geosciences*, 5(3):225–256, 2001.
- [27] C.E. Schaerer, D. Marchesin, M. Sarkis, and P. Bedrikovetsky. Permeability hysteresis in gravity counterflow segregation. *SIAM Journal on Applied Mathematics*, 66(5):1512–1532, 2006.
- [28] B. Schweizer. The Richards equation with hysteresis and degenerate capillary pres-

- sure. *Journal of Differential Equations*, 252(10):5594 – 5612, 2012.
- [29] B. Schweizer. Hysteresis in porous media: Modelling and analysis. *Interfaces and Free Boundaries*, 19(3):417–447, 2017.
- [30] M. Shearer, K.R. Spayd, and E.R. Swanson. Traveling waves for conservation laws with cubic nonlinearity and BBM type dispersion. *Journal of Differential Equations*, 259(7):3216–3232, 2015.
- [31] K. Spayd and M. Shearer. The Buckley–Leverett equation with dynamic capillary pressure. *SIAM Journal on Applied Mathematics*, 71(4):1088–1108, 2011.
- [32] C.J. van Duijn and J.M. de Graaf. Large time behaviour of solutions of the porous medium equation with convection. *Journal of differential equations*, 84(1):183–203, 1990.
- [33] C.J. van Duijn, Y. Fan, L.A. Peletier, and I.S. Pop. Travelling wave solutions for degenerate pseudo-parabolic equations modelling two-phase flow in porous media. *Nonlinear Analysis: Real World Applications*, 14(3):1361–1383, 2013.
- [34] C.J. van Duijn, K. Mitra, and I.S. Pop. Travelling wave solutions for the Richards equation incorporating non-equilibrium effects in the capillarity pressure. *Nonlinear Analysis: Real World Applications*, 41(Supplement C):232 – 268, 2018.
- [35] C.J. van Duijn, L.A. Peletier, and I.S. Pop. A new class of entropy solutions of the Buckley–Leverett equation. *SIAM Journal on Mathematical Analysis*, 39(2):507–536, 2007.
- [36] L. Zhuang. *Advanced theories of water redistribution and infiltration in porous media: experimental studies and modeling*. PhD thesis, University of Utrecht, Dept. of Earth Sciences, 2017.